A Promising Approach to Obtain Excellent *n*-Type Organic Field-Effect Transistors — Introducing Pyrazine Ring

Xian-Kai Chen,[†] Jing-Fu Guo,[‡] Lu-Yi Zou,[†] Ai-Min Ren[*,†] and Jian-Xun Fan[†]

† State Key Laboratory of Theoretical and Computational Chemistry, Institute of Theoretical Chemistry, Jilin University, Changchun 130023, China
‡ School of Physics, Northeast Normal University, 130024, P. R. China
Correspondence to: A.-M. Ren; e-mail: **aimin_ren@yahoo.com**

The effects of pyrazine ring on the geometrical and electronic structures, molecular stacking motifs, carrier injection and transport properties as well as electronic band structures for some typical molecules with pyrazines (such as tetracene, pentacene and π-extended TTF derivatives) were theoretically investigated by quantum chemical methods. The introduction of pyrazine doesn't affect the molecular planarity, in the meantime, largely decreases the energies of the highest occupied molecular orbitals (HOMOs) and the lowest unoccupied molecular orbitals (LUMOs), and hence improves their stability in air and ability of electron injection. More important, it is very helpful for prompting the molecular π-stacking. Small electron reorganization energies and large electronic coupling originated from their dense π-stacking give rise to their excellent electron transport properties, which makes them become a class of promising candidates for excellent *n*-type organic field-effect transistor (OFET) materials. So introducing pyrazine is an effective approach to obtain the excellent n-type

OFET materials.

1. Introduction

Organic π-conjugated materials are of immense interests. They have been extensively investigated for optoelectronic and microelectronic applications, such as organic light-emitting diodes (OLEDs),[1,2] organic field-effect transistors (OFETs),[3-5] or organic photovoltaic devices (OPVs),[6,7] which are often called as organic semiconductors. Recent progresses have shown that some typical organic semiconductors have achieved mobility beyond $10 cm^2 V^{-1} s^{-1}$ (such as pentacene and rubrene),[8,9] which can even be compared with the mobility of amorphous-silicon devices. To make full use of organic electronic circuitry, it is very necessary to combine *p*-type and *n*-type transistors to produce complementary circuits which show far greater speed, reliability, and stability than those of unipolar circuits. So the development of high-performance *n*-type semiconductors is strongly required for the fabrication of organic *p-n* junctions. In the past several decades, most efforts were devoted to *p*-type organic semiconductors,[8,10-18] whereas the development of *n*-type ones lagged behind. The primary reason is due to high injection barrier of electron and the intrinsic instability of organic radical anions in air, something which can be overcome by increasing the electron affinity.[5,19] Recently, experimental and theoretical studies showed

that functionalizing *p*-type semiconductors with electron-withdrawing groups was a promising way to convert them into *n*-type ones, such as the cyanation[20-23](-CN) or halogenation[24-27](-Br, -Cl and -F). But these substituents give rise to the distortion of some planar molecules (such as PBI-FCN2, PBI-F$_4$ or the halogenated tetracene derivatives),[27,28] which is adverse to strong π-orbital overlap between adjacent organic molecules in solid state and hence weakens their carrier transport performance. To develop high-performance *n*-type organic semiconductors, new molecular designs need to be explored.

Bunz et al demonstrated that the oligoacenes with pyrazine rings should be promising candidates for excellent *n*-type OFETs because of their large electron affinities and various intermolecular interactions.[29-30] Yamashita et al also found similar properties for diindenopyrazinedione derivatives and π-extended TTF derivatives (4-9 and 5-11 in Figure 1, respectively).[31,32]Recently, Miao's group for the first time reported that the pentacene derivatives (3-6/7 and 6-12/13 in Figure 1) were applied to *n*-type OFETs and investigated their electronic structures, molecular packing and semiconductor properties.[33-35]Their research results indicated that molecule 3-7 exhibited the electron mobility up to 3.3cm^{2}V^{-1}s^{-1},[33]which made it become one of the best promising *n*-type organic semiconductor materials. They considered that the high electron mobility may be attributed to its low LUMO energy level and dense

packing of molecules in a 2-D brickwork arrangement. In the theoretical investigations, Houk et al detailedly investigated their structures, electron affinities, excitation, ionization, and reorganization energies for the oligoacenes with pyrazine.[36] Their results showed that some molecules possessed large electron affinities (up to 3eV) and small electron reorganization energies (<0.20eV) making these compounds become promising candidates for *n*-type semiconducting materials. Unfortunately, the effects of the pyrazine on their molecular stacking motifs, carrier mobilities and electronic band structures were not investigated in the paper.

In the study, we systematically investigate the effects of pyrazine ring introduced on their geometrical and electronic structures, molecular stacking motifs, carrier injection and transport properties as well as electronic band structures for the typical molecules presented in Figure 1 by theoretical methods from the following aspects, such as:

(1) the introduction of pyrazine ring,

(2) the increase of pyrazine introduced,

(3) the position of pyrazine introduced.

Through our theoretical study, the intrinsic transport behavior for these excellent *n*-type semiconductor materials with pyrazine ring is revealed, which can provide a fertile theoretical ground with the rational molecular design and synthesis of the desired *n*-type OFET materials.
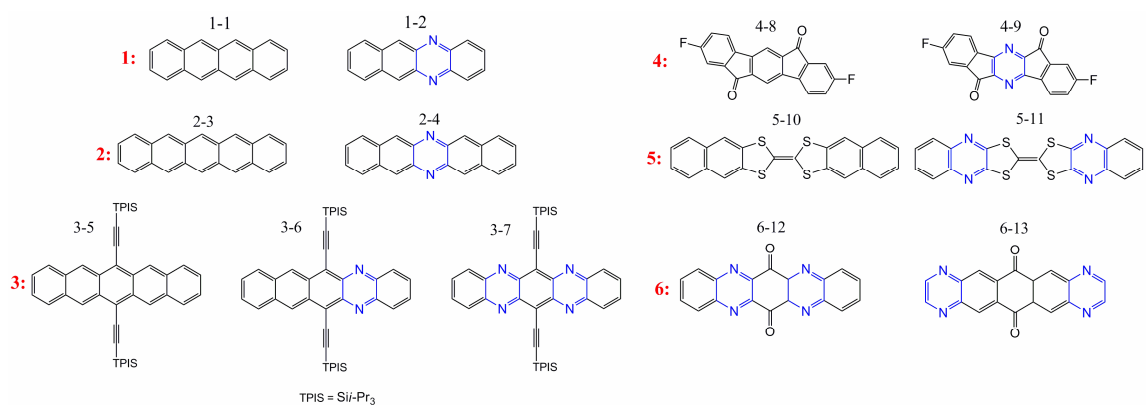
Figure 1. Chemical structures of the compounds investigated in this study

2. Theoretical and Computational Method

There are mainly two types of carrier transport mechanisms in organic electronic materials: (1) the coherent band mechanism and (2) the incoherent hopping mechanism.[37-42] In low temperature, the band mechanism dominates for highly-ordered organic crystals. The carrier moves as a highly delocalized plane wave in an energy band.[42] The interaction between the nearest-neighbor molecules is large compared with dynamic structural disorder, for instance, reorganization energies resulting from charge transfer process from one molecule to another.[40-41] At high temperature (probably at room temperature) or in polycrystalline (or less-ordered) systems, intermolecular interactions are mainly from weak *van der Waals* forces, in which charge carriers are expected to be localized over a single molecule and thus the band mechanism may be invalid.[42] The transport mechanism can be described here in terms of sequential jumps of the relaxed charges between adjacent molecules, that is, the mechanism can

be referred to as hopping mechanism. Extensive experimental evidences, particularly the observed thermal signatures and optical spectra are consistent with this assumption.[43-46]

Here, each hopping event is viewed as a non-adiabatic charge transfer reaction *i.e.* the charge transport process between two adjacent molecules follows the reaction $M+M^{+/-}=M^{+/-}+M$ (see Figure 2(a)). Charge transfer rate between neighboring molecules can be expressed by standard Marcus theory by the following equation:[47]

$$k_{ct} = \frac{4\pi^2}{h} \frac{V^2}{\sqrt{4\pi\lambda k_B T}} \exp\left\{-\frac{\lambda}{4k_B T}\right\} \tag{1}$$

Where λ is the reorganization energy, and V is transfer integral between the two species M and $M^{+/-}$, T is the temperature and k_B is the Boltzmann constant.
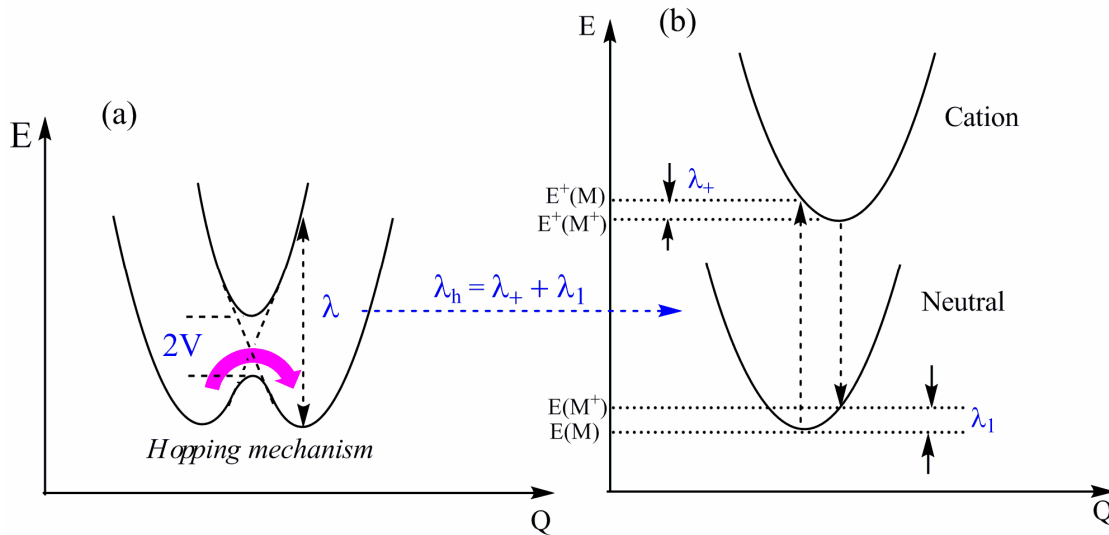

Figure 2. (a) Schematic representation of a charge exchange reaction pathway for hole transfer through a transition state by weak (nonadiabatic) coupling. The solid curves are the adiabatic surfaces, while the dashed lines

refer to diabatic surfaces. (b) Schematic description of internal reorganization energy for hole transfer. The reaction coordinate Q is an ensemble of geometric modifications of the dimer system.

Here, charge transport is modeled as a Brownian motion process, as described by a particle diffusion process. The mobility can be obtained by the Einstein equation:[48]

$$\mu = \frac{e}{k_B T} D \qquad (2)$$

Where μ is the carrier mobility, D is the isotropic charge diffusion coefficient, and e is the electronic charge. Given the hopping rate between the nearest-neighbor molecules, the diffusion coefficient can be evaluated from the hopping rates as

$$D = \frac{1}{2n} \sum_i r_i^2 k_i P_i \qquad (3)$$

where n is the dimensionality(when n is equal to 3, we can evaluate the average mobility of all the hopping pathways), k_i is the hopping rate due to charge carrier to the ith neighbor, r_i is the distance to neighbor i, P is the relative probability for charge carrier to a particular ith neighbor,

$$P_i = k_i / \sum_i k_i \qquad (4)$$

Summing over all possible hops leads to the diffusion coefficient in equation (3)

From equation (1), charge transfer rate is mainly determined by two

important parameters: reorganization energy (λ) and transfer integral (V).

Here, the reorganization energies (λs) are evaluated directly from the

adiabatic potential-energy surfaces of neutral/cation or neutral/anion

species (see Figure 2(b)). λ_h for hole can be defined as follows

$$\lambda_h = \lambda_+ + \lambda_1 = \left[E^+(M) - E^+(M^+)\right] + \left[E(M^+) - E(M)\right] = IP(v) - HEP \qquad (5)$$

As illustrated in Figure 2(b), $E^+(M^+)$ and $E(M)$ represent the energies of

the cation and neutral species in their lowest energy geometries,

respectively., while $E^+(M)$ and $E(M^+)$ represent the energies of cation and

neutral species with the geometries of neutral and cation respectively. In

this way, λ_e for electron can be expressed as follow

$$\lambda_e = \lambda_- + \lambda_2 = \left[E^-(M) - E^-(M^-)\right] + \left[E(M^-) - E(M)\right] = EEP - EA(v) \qquad (6)$$

It is well known that B3LYP functional is widely applied to the

calculations of the geometrical optimization, ionization potentials, electron

affinities and reorganization energies.[23,28,40-41,49-50] So the monomer

geometries of the neutral and ion states of all the studied molecules were

fully optimized by the B3LYP functional and unrestricted formalism

(UB3LYP) coupled with 6-31G(d,p) basis set, respectively.[28,49,50]

Following each optimization, the vibrational frequencies were calculated

and the results showed that all optimized structures were stable geometric

structures without imaginary vibration frequency. To characterize the

energies of these species studied more accurately, a single point calculation

on every specie was carried out at the B3LYP/6-31++G(d,p) level.[28,50] On

the basis of the above calculations, the corresponding ionization potentials (IP), electron affinities (EA), hole extraction potentials (HEP), electron extraction potentials (EEP) and the reorganization energies (λ) were obtained. The calculations of the above quantities were performed using the GAUSSIAN09 program package.[51]

The transfer integrals (V) for the nearest-neighbor dimers along the transfer pathways in their crystals were calculated by using a fragment orbital approach[52] in combination with a basis set orthogonalization procedure.[53] Transfer integral can be calculated from the spatial overlap (S_{RP}), charge transfer integral (H_{RP}) and site energies (H_{RR}, H_{PP}). Transfer integral V is given by equation (7):

$$V = \frac{H_{RP} - 0.5S_{RP}(H_{RR} + H_{PP})}{1 - S_{RP}^2} \qquad (7)$$

where $H_{RP} = \langle \psi_R | H | \psi_P \rangle$, $H_{RR} = \langle \psi_R | H | \psi_R \rangle$, $H_{PP} = \langle \psi_P | H | \psi_P \rangle$ and $S_{RP} = \langle \psi_R | \psi_P \rangle$; H is the system Kohn-Sham Hamiltonian of the dimer system, and $\Psi_{R(P)}$ means the monomer's LUMO (for electron transport) with Löwdin's symmetric transformation, which can be used as the orthogonal basis set for calculation.[42] All the calculations of transfer integral were performed with PW91/TZ2P method,[49-50,54] using the ADF (Amsterdam density functional) package.[55] The study of Huang et al. showed that PW91 functional gave the best description for the bandwidth of organic solid[54] and some groups et al also obtained very good results using PW91/TZ2P method in the similar investigations.[49-50]

To investigate the anisotropy of carrier transport in the crystals, the calculations of their electronic band structures were performed by the Perdew–Burke–Ernzerhof (PBE) exchange-correlation functional[56] and an all-electron double numerical basis set with polarized function (DNP basis set) using Dmol3 within the Material Studio package.[57,58] All the calculations were based on the crystal structures without geometry optimization with a Monkhorst–Pack mesh[59] of 10×10×10 k-points.

3. Results and Discussion

Reorganization Energies: a)Geometries: All the molecular geometries optimized exhibit the planar and rigid skeletons. To clarify the effect of pyrazine ring on the geometries of the studied molecules, the series molecules 3 and 6 are taken as the examples and their corresponding neutral structural parameters are shown in Figure 3. For molecules 3-6 and 3-7, the introduction of pyrazine and its increase slightly affect other structures compared with molecule 3-5. The substitutions of C-H bonds by nitrogen atoms possessing strong electron-withdrawing ability lead to the reduction of the corresponding intra-ring (pyrazine ring) bond lengths to 1.33/1.35Å and bond angles to 117.8°. For series molecules 6, the position of pyrazine ring has little effect on the corresponding bond angles, while other bond lengths for molecule 6-12 are larger than the corresponding values for molecule 6-13 except bond C=O.
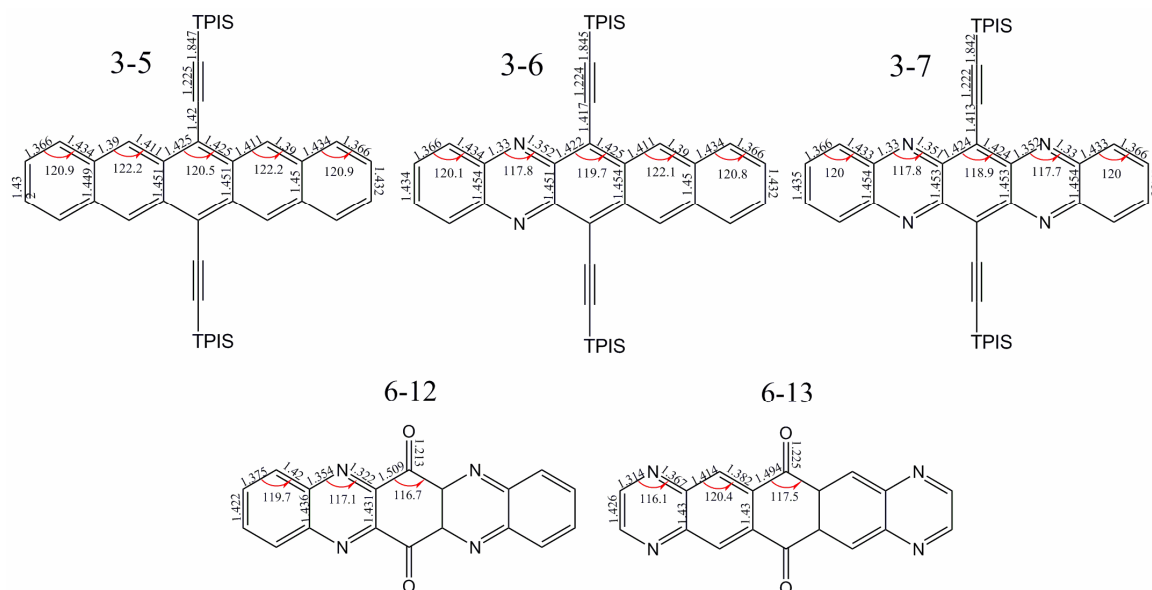
Figure 3. Structural parameters (bond angle/°; bond length/Å) of their neutral geometries optimized for series molecules 3 and 6

The reorganization energy is originated from the geometrical relaxation accompanying charge transfer process from one molecule to another. From Figure 2, it can be found that hole (electron) reorganization energies are closely related to the geometries of cation (anion) states. The reorganization energies are in proportion to the deformation of the geometries in charge transfer process.[60] The changes of bond lengths between the neutral and ionized geometries for series molecules 3 and 6 are presented in Figure S1. For series molecules 3, the largest deformations of bond lengths both for cation and anion geometries appear on the bond C-Si, on the order of 0.025Å and 0.029Å, respectively. And the sums of the absolute values of bond lengths changes for 3-5, 3-6 and 3-7 are 0.176Å, 0.189Å and 0.202 Å (for cation) and 0.201Å, 0.204Å and 0.220Å (for

anion), respectively. It can be found their geometrical deformations accompanying electron transfer are larger, so the electron reorganization energies for series molecules 3 should be larger than the corresponding hole ones, and molecule 3-7 probably possesses the largest reorganization energies due to its largest geometrical deformation. From Figure S1, the deformations on the middle benzenes (bond index 6, 7, 10, 18 and 19) possess large differences among series molecules 3. To explain it, the contribution of every atom to the corresponding highest occupied molecular orbital (HOMO) and lowest unoccupied molecular orbital (LUMO) for series molecules 3 and 6 is presented in Figure 4. The larger contribution of atom to HOMO and LUMO should lead to larger deformation on these structures adjacent to it in charge transfer process.[22] From Figure 4, the largest contributions to their HOMOs and LUMOs are from the central C atoms adjacent to alkynes for 3-5, 3-6 and 3-7, and their contributions have obvious differences among these molecules. For series molecules 6, due to large contributions of pyrazine ring to HOMOs and LUMOs, the dominant geometrical deformations focus on pyrazine rings.
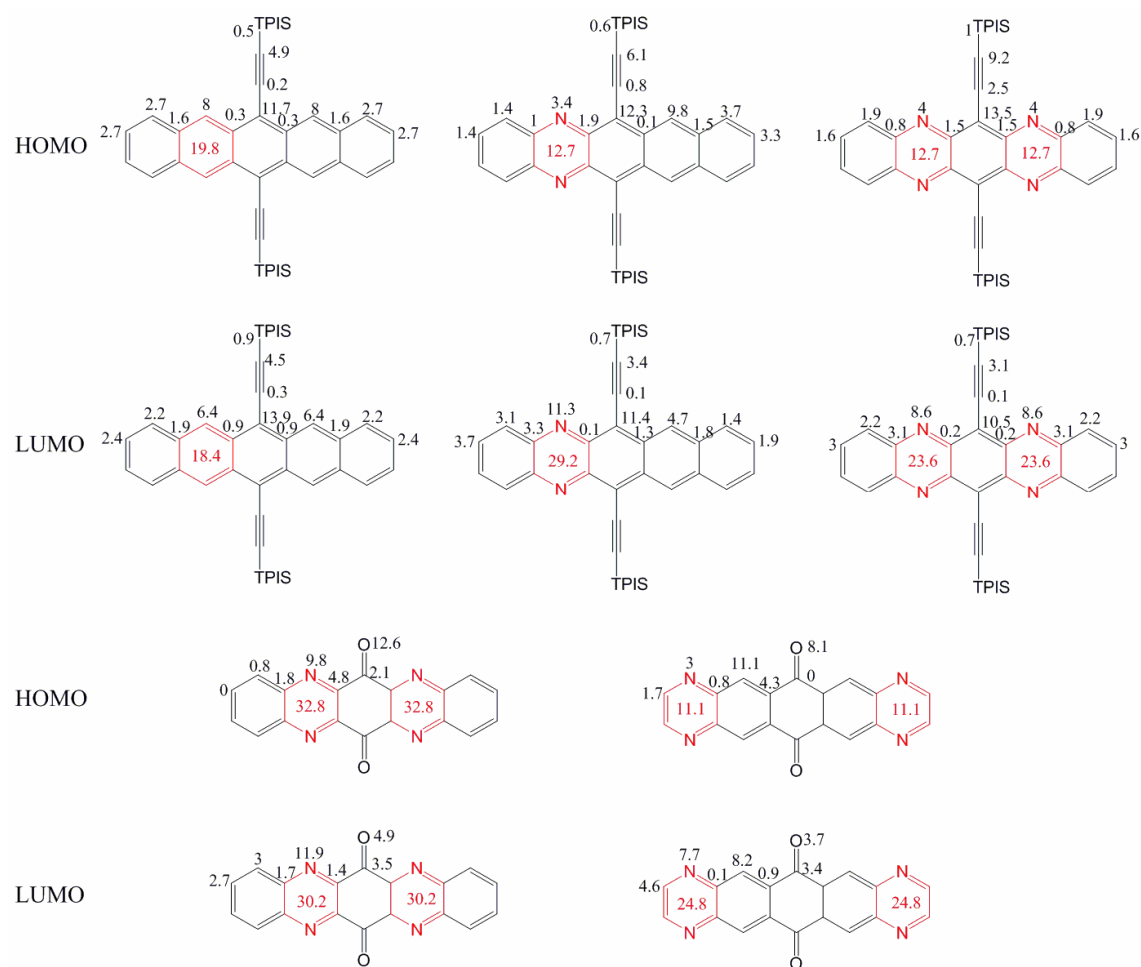
Figure 4. Contribution (%) of every atom to their HOMOs and LUMOs for series molecules 3 and 6; red figures denote the contributions (%) of those structures marked by red to their corresponding HOMOs and LUMOs.

b) Frontier Molecular Obitals, Ionization Energies and Electron Affinities: It will be useful to examine the HOMO and LUMO levels of the studied molecules. The reorganization energy (the description of local electron-vibration coupling in charge transfer process) is closely related to molecular HOMO and LUMO.[42]The relative orderings of HOMOs and

LUMOs energies provide a reasonable qualitative indication of the ability of hole and electron injection, respectively. The energies of HOMOs and LUMOs of all the studied molecules and their corresponding electronic density contours are shown in Figure 5.

From Figure 5, the electronic density of all the studied molecules mainly distributes in their whole rigid π-conjugated skeletons. It can be found that the introduction of pyrazine ring is helpful to stabilize the HOMOs and LUMOs of the studied molecules, in the meantime, has little effect on the energy differences between the corresponding HOMOs and LUMOs except for series molecules 5. For the molecules with pyrazines, their HOMO and LUMO levels are very low within the range -7.18～-4.97eV and -3.49～ -2.23eV, respectively. Introducing pyrazines is adverse to hole injection because their low HOMO energies and hence large ionization energies in terms of Koopmans' theorem. To understand the role of pyrazine rings in their HOMOs and LUMOs more quantitatively, taking series molecules 3 and 6 as the examples, the contributions of pyrazine rings to their corresponding HOMOs and LUMOs are presented in Figure 4. Our result indicates that for these molecules, the contributions of pyrazines to their LUMOs are larger than those of benzenes substituted and hence decrease their LUMOs energies. With the increase of introduced pyrazines from molecules 3-5 to 3-7, their HOMO and LUMO energies continuously decrease. For series molecules 6, the position of pyrazines strongly

influences their frontier molecular obitals. The contribution of pyrazines to its LUMO for molecule 6-12 is larger than that for molecule 6-13, so the former possesses lower LUMO level and hence better electron injection ability. In this case that the interfacial vacuum energy shift is neglected, the energy barrier of electron (hole) injection from the electrode to the organic semiconductor is the energy difference between the electrode's work function and LUMO (HOMO) energy level of the organic material (the injection barrier $\Phi_B=\Phi_m$-|LUMO| (Φ_m: the work function of the metal electrode) for electron injection; Φ_B=|HOMO|-Φ_m for hole injection).[61] In the experiments, Au with a work function of about 5.1eV in vacuum is widely applied to the electrode of OFETs[61] and thus acted as the source and drain electrodes in our case. Although the apparent energy differences between Au and organic semiconductors are often larger than 1 eV, it is still beneficial to the injection of electrons into the LUMO levels in a certain extent. In fact, most of the researches involving n-channel OTFTs using Au as electrode show that they have a much higher performance than those using other metals[61]. As expected by us, their electron injection barriers are larger than the corresponding hole ones. But compared with other promising *p*-channel OFET materials (such as: oligoacenes and oligothiophenes), the studied molecules with pyrazine are not suitable for *p*-channel OFET materials due to their low HOMO levels. In contrary, they possess low barriers of electron injection due to their low LUMO levels,
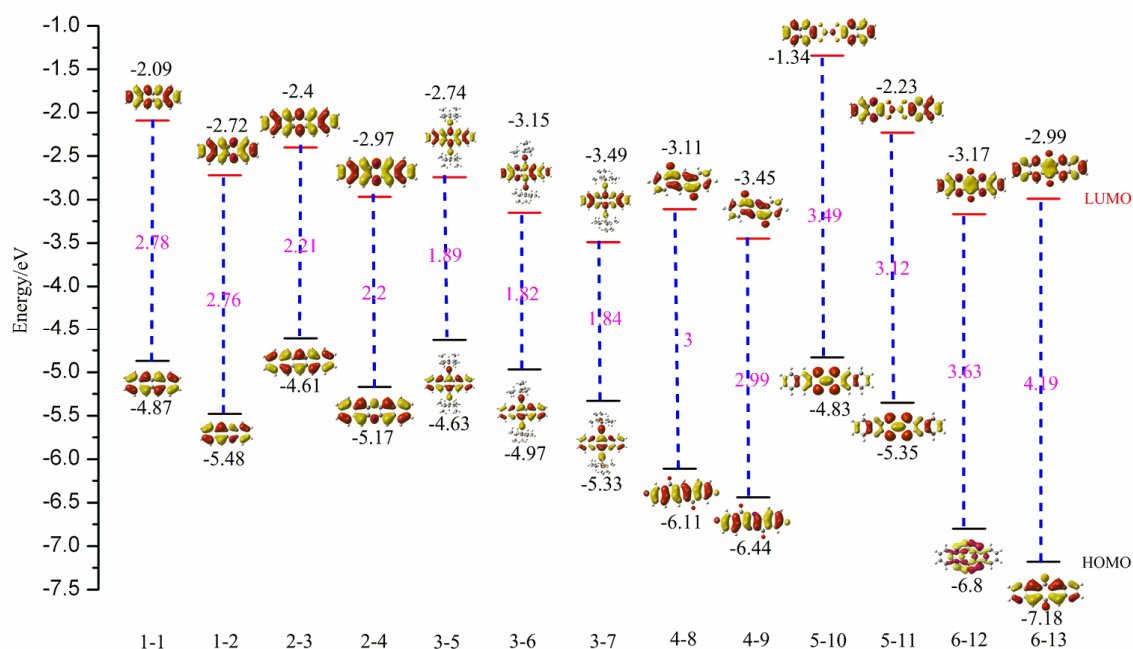
Figure 5. The energies of HOMOs and LUMOs of all the studied molecules and their electronic density contours

Thus, IP and EA values are calculated and Table 1 contains the ionization potentials (IPs), electron affinities (EAs), both vertical (v; at the geometry of the neutral molecule) and adiabatic (a; optimized structure for both the neutral and charged molecule), and extraction potentials (HEP and EEP for the hole and electron, respectively) that refer to the geometry of the ions.

values due to their low LUMO and HOMO levels. Their large EA(v) values give rise to high stability of their radical anions in ambient atmosphere, which is an important requirement of fine *n*-type OFET materials. In contrary, their large IP(v) values probably weaken the stability of their radical cations in air for *p*-type OFETs. Recently, some investigations have shown that intermolecular interactions have large effect on their frontier molecular orbitals, IPs and EAs and etc for the studied molecules.[62-64] To understand it in our case, molecules 6-12 and 6-13 are taken as the examples. Our result indicates that the intermolecular interactions indeed largely influence the absolute values of the above quantities, but they should possess little effect on evaluating the relative performances of these molecular materials by the above parameters obtained at single-molecule level. (the detail is in Supporting Information).

From Table 1, the introduction of pyrazine slightly increases electron (hole) reorganization energies by 0.01～0.06(0.04)eV, which doesn't largely affect their charge transfer rate. As predicted in the "Geometries" section, with the increase of pyrazine rings from 3-5 to 3-7, the reorganization energies slightly increase. Because the electron reorganization energies for other molecules studied are below 0.2eV except for series molecules 4 and their fine electron injection ability, introducing pyrazine should be an effective way to obtain excellent *n*-type OFET materials. To further demonstrate it, their crystal stacking motifs, transfer integrals and electron

mobilities for the molecules with pyrazine rings will be detailedly discussed in the following section.

TABLE 1: Ionization Potentials (IPs), Electronic Affinities (EAs), Extraction Potentials and Reorganization Energies (λs) of the studied molecules (in eV)

Species	IP(v)	IP(a)	HEP	EA(v)	EA(a)	EEP	λ_{hole}	λ_{elec}
1-1	6.56	6.51	6.45	1.01	1.10	1.17	0.11	0.16
1-2	7.21	7.15	7.09	1.61	1.70	1.79	0.12	0.18
2-3	6.17	6.13	6.08	1.42	1.49	1.55	0.09	0.13
2-4	6.76	6.72	6.68	1.97	2.04	2.12	0.08	0.15
3-5	5.97	5.90	5.84	1.94	2.03	2.13	0.13	0.19
3-6	6.31	6.22	6.14	2.33	2.42	2.53	0.17	0.20
3-7	6.65	6.54	6.44	2.66	2.76	2.87	0.21	0.21
4-8	7.84	7.72	7.55	2.12	2.29	2.43	0.29	0.31
4-9	8.19	8.06	7.89	2.43	2.62	2.80	0.30	0.37
5-10	6.31	6.20	6.09	0.52	0.6	0.66	0.22	0.14
5-11	6.84	6.73	6.61	1.36	1.46	1.55	0.23	0.19
6-12	8.62	8.42	8.25	2.22	2.28	2.35	0.37	0.13
6-13	8.91	8.71	8.52	2.06	2.14	2.21	0.39	0.15

The suffixes (v) and (a) respectively indicate vertical and adiabatic values

Molecular Stacking Character, Transfer Integral and Carrier Mobility: It is well known that charge transport properties of OFETs are highly sensitive to the relative orientations and crystal stacking characters of organic molecules involved.[65-67]Many small molecules, the most promising *p*-type OFETs, such as, oligoacences, TTF and oligothiophenes and etc, show a herringbone packing motif.[42]This packing motif does not provide optimal intermolecular π-orbital overlap, which is a critical factor affecting the transfer integral and hence intrinsic carrier

mobility.[42]Therefore, some research groups have attempted to obtain their derivatives possessing the π-stacking motif by functionalizing the above molecules, but the way probably gives rise to the distortion of the plane molecular skeleton.[20-27]Recently, introducing pyrazine into the above small molecules is an exciting molecular design that effectively inverts the herringbone packing to the π-stacking and doesn't affect the molecular planarity.[31-35]Taking the molecules 1-1/2, 3-6/7, 5-10/11 and 6-12/13 as the examples, their crystal stacking motifs are presented in Figure 6.
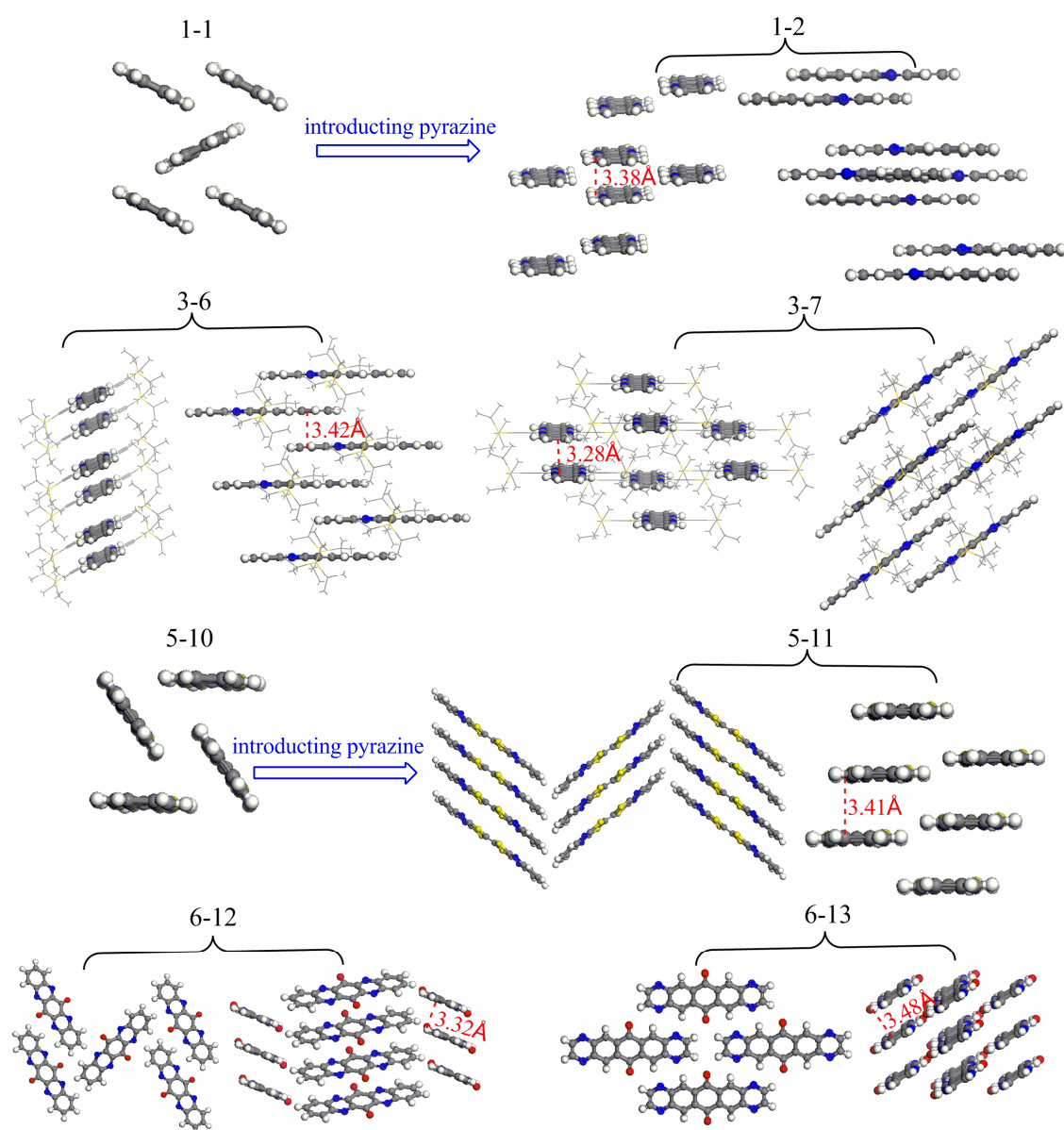
Figure 6. Crystal stacking for molecules 1-1/2, 3-6/7, 5-10/11 and 6-12/13; the bracket denotes the stacking motif from different views.

We find molecules 1-1 and 5-10 exhibit typical herringbone packing. Once the benzenes are substituted by the corresponding pyrazine rings, the crystal stacking motif is inverted to the π-stacking of molecules 1-2 and 5-11 which is more beneficial for carrier transport. From Figure 6, molecules 3-6/7 and 6-12/13 also show dense molecular π-stacking. Although the π-stacking of series molecules 3 is mainly originated from

their large triisopropylsilyl substituents (TPIS),[33,68-69] with the introduction and increase of pyrazine rings from 3-5 to 3-7, their minimal inter-plane separations exhibit the reduction trend from 3.47Å to 3.28Å. This indicates that their introduction should give rise to stronger intermolecular interactions and hence reduce the separations. From Figure 6, it can be found that the minimal inter-plane separations for the molecules with pyrazines are within *van der Waals* radius (3～4Å) and are close to that (3.35Å) for graphite. It is necessary to be pointed out that the π-stacking also appears in single crystals of pyrazine and anthracene derivative with pyrazine, but pyridine and anthracene derivative with pyridine don't show the π-stacking character in their crystals (Crystallographic data were retrieved from the Cambridge Structural Database). It illuminates that the π-stacking in these molecular crystals should be attributed to the character of pyrazine ring, but not only the introduction of N atom. In the meantime, the effects of the 2nd N atom of pyrazine on electronic structures, IPs, EAs and λs of the similar molecules have been detailedly investigated by Houk et al.[36] And the same conclusions are also obtained in our case (in Supporting Information). The molecular crystal packing is determined by different types of intermolecular interactions between the molecules. For our systems studied, the π-π interactions and H-bond interactions arising from N atoms widely exist. Therefore, knowing the binding energies between the molecules is very helpful to understand the molecular packing

of organic crystals. To clarify the reason why the π-stacking of the above molecules forms, the dimer model for molecule 1-2 is taken as the example and the binding energies of the dimers with different torsion angles (θ) are calculated by using the following equation:

$$\Delta E = E_{\dim er} - 2E_{monomer} \qquad (8)$$

Where E_{dimer} is the total energy of the dimer, $E_{monomer}$ is the energy of an isolated monomer and $\varDelta E$ is the binding energy of the corresponding dimer. Meanwhile, basis set superposition error (BSSE) was taken into account by using a counterpoise correction scheme. The model and the calculated results are presented in Figure 7 (a) and (b), respectively. These calculations of binding energies were performed by M06-2X/6-311+G(d,p) within the GAUSSIAN09 program package. M06-2X functional is considered to be suitable for the description of non-covalent interactions such as π-π interaction and H-bond interaction, and cheaper than MP2 and CCSD.[28,70-71]Noted that in the case of the π-stacking benzene dimer, two-body effects dominate the binding energy, the contribution only 10% of the addition third and fourth benzenes to the total binding energy (normalized for the number of benzenes).[70,72]From Figure 7(b), it can be found that the face-to-face π-stacking both for *cis-* and *trans-* dimers possesses the strongest intermolecular interaction and it continuously weakens with the increase of torsion angle from 0° to 90°, which illuminates the rationality of the π-stacking for the molecules with

pyrazines. In addition, it is noted that the head-to-tail arrangement (*trans*-dimers) for molecule 1-2 possesses stronger intermolecular interaction, which is accordant with its actual crystal packing, and molecule 3-6 also exhibits the same arrangement in its crystal. It should be main reason that for the head-to-tail π-stacking, the negative charged N atoms of pyrazine in one monomer and electropositive π-aromatic benzene in another monomer possess strong electrostatic attraction.
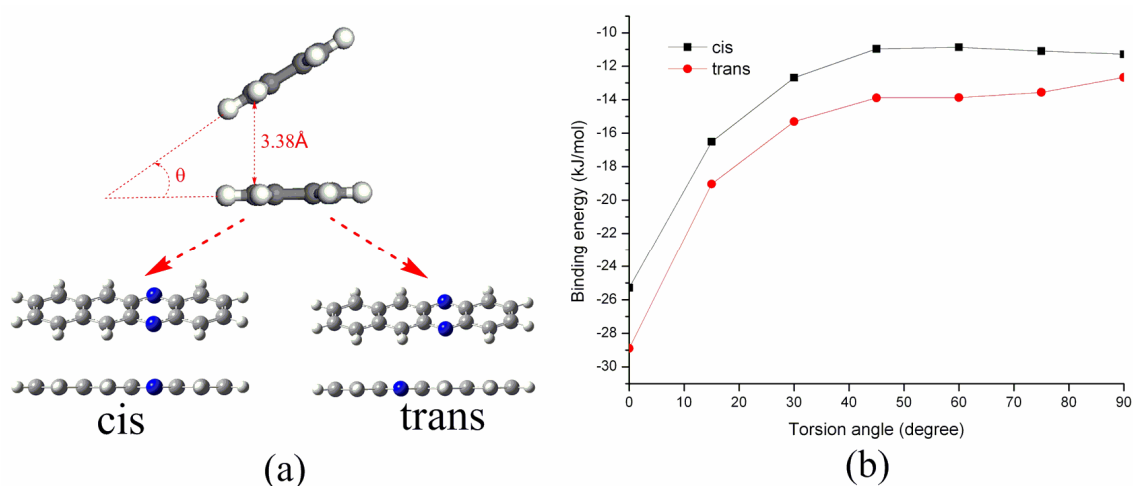

Figure 7. (a) the rotation of one monomer around the molecular long axis with the torsion angle θ from 0° to 90° in the interval of 15° at a fixed 3.38Å (the minimal inter-plane distance for the crystal packing of molecule 1-2) molecular edge-to-edge distance. "cis(trans)" denotes two monomers are in the head-to-head(tail) arrangement. (b) the binding energies calculated for the cis/trans-dimers as the function of torsion angles.

The π-stacking character probably gives rise to fine π-orbital overlap and hence large transfer integral value. Taking molecules 1-2, 3-6/7 and 6-12/13 as the examples, all the identified nearest-neighbor hopping

pathways for these molecules are presented in Figure 8 and the corresponding transfer integral values calculated by equation (7) are listed in Table 2. It can be found that the π-stacking of these molecules indeed leads to large transfer integral values, and the maximal V values for molecules 3-6/7 and 6-12/13 appear on the dimers possessing the minimal inter-plane distances except for molecule 1-2. To observe the overlap of π orbitals of the above interacting molecules, the LUMOs of the corresponding dimers possessing the maximal V values are presented in Figure 9. The transfer integral is increased if both are bonding or anti-bonding interactions between the π-atomic orbitals and decreased when there occurs a cancellation between bonding and anti-bonding overlaps.[43] From Figure 9, it can be seen that the wave functions of the interacting monomers for molecules 1-2, 3-6 and 6-12/13 at the overlapping region possess the same phase, and thus these dimers exhibit optimal π-orbital overlap and large V values. Here, the dimer for molecule 3-7 is an exception, where a cancellation between bonding and anti-bonding overlaps weakens the electronic coupling between the interacting molecules and hence decreases the corresponding V value. From Table 2, it is noted that for molecule 1-2, the V value for dimer possessing the minimal inter-plane separation (3.38Å) along pathway 1 is smaller than that for the dimer with the inter-plane separation (3.48 Å) along pathway 3. To illuminate the reason, the molecular packing motifs

and LUMOs of the dimers along the pathways 1 and 3 are shown in Figure 10. It can be clearly seen that the dimer along the pathway 1 possesses a replacement of about half a benzene ring width, which gives rise to a cancellation between bonding and antibonding overlaps and hence smaller V value. In contrast to pathway 1, the packing motif of the dimer along the pathway 3 leads to full bonding or antibonding interactions between the π orbitals and thus stronger electronic coupling. Comparing their V values for molecules 3-6 and 3-7, lower LUMO level of molecule 3-7 caused by the increase of pyrazine introduced doesn't improve its electron transport property, because its increase largely also changes the molecular stacking which doesn't lead to optimal π-orbital overlap. In addition, it should be noted that their dominant transfer pathways for the crystals of molecules 3-6 and 3-7 appear in the a-b plane, and the inter-layer carrier transport isn't effective. In combination with the following analysis of charge-transport anisotropy, it can be understood that their molecular crystals exhibit the 2-D transport character. From Tables 1 and 2, it can be found that compared with molecule 6-13, smaller electron reorganization energy (0.13eV) for molecule 6-12 doesn't lead to larger electron mobility. It should be main reason that the position change of pyrazines inverts *P21/N* space group of molecule 6-12 crystal to *C2/M* space group of molecule 6-13 crystal, which makes molecule 6-12 crystal not possess large transfer integral.
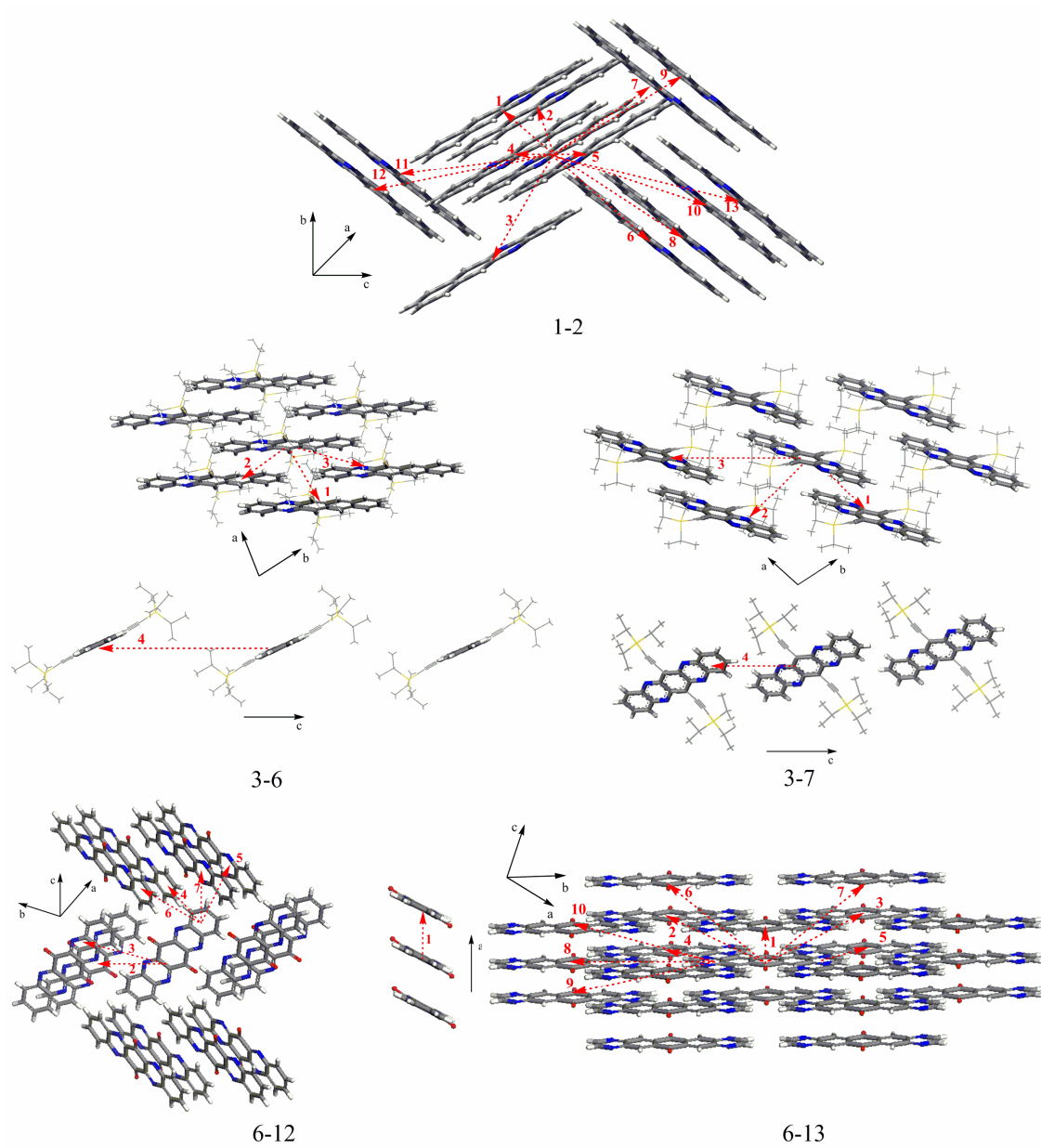
Figure 8. Charge hopping pathways schemes for molecules 1-2, 3-6/7 and 6-12/13; Due to symmetry, the reverse pathways aren't labeled for molecules 3-6/7 and 6-12/13.

TABLE 2: Electron transfer integrals (V_e/meV) for molecules 1-2, 3-6/7 and 6-12/13 along different hopping pathways calculated (P: the hopping pathway; d/Å: the mass center distance). μ_e/cm^{2}V^{-1}s^{-1} is the average electron mobility.

P	1-2		3-6		3-7		6-12		6-13	
	V_e	d	V_e	d	V_e	d	V_e	d	V_e	d
1	35.85	3.72	-1.30	7.66	-57.12	8.06	-75.69	3.89	-156.97	3.8
2	1.83	6.81	-101.34	7.72	0.59	10.51	5.66	9.07	-2.16	9.61
3	51.6	6.95	50	10.07	0.26	14.47	-0.29	9.87	-2.16	9.61
4	-4.11	7.07	0.04	16.98	-2.27	12.76	-5.86	10.39	-0.09	10.14
5	-4.11	7.07					-5.86	10.39	-0.09	10.14
6	5.16	8					2.69	10.53	-0.63	10.52
7	5.16	8					2.69	10.53	-0.63	10.52
8	28.25	9.19							14.04	16.04
9	28.25	9.19							-3.08	16.48
10	0.24	9.48							-3.08	16.48
11	0.24	9.48								
12	7.93	11.31								
13	7.93	11.31								
μ_e	0.67		1.92		0.72		0.79		2.49	
					$(1.0\text{-}3.3, 0.3\text{-}0.5)^{34}$		$(0.04\text{-}0.12)^{35}$			

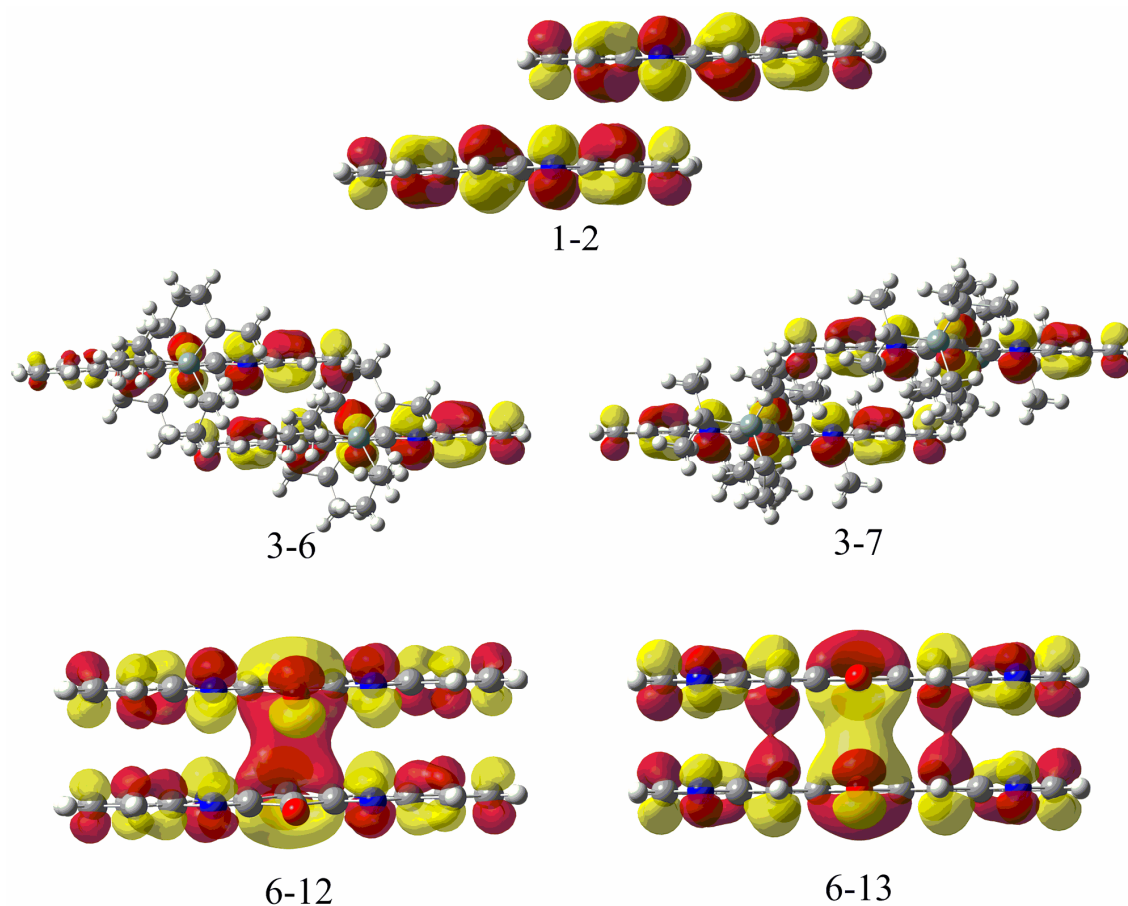The data in the bracket are the experimental results.

Figure 9. LUMOs of the corresponding dimers along the transfer pathways possessing the maximal V values for molecules 1-2, 3-6/7 and 6-12/13.
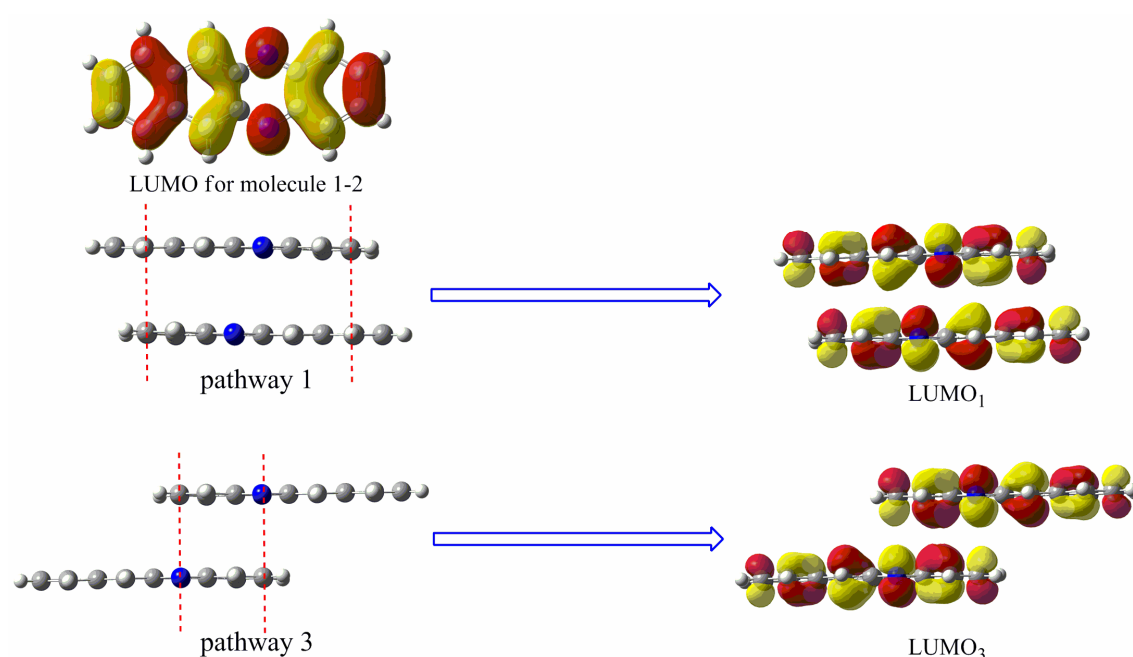
Figure 10. The molecular packing motif and $LUMO_{1(3)}$ of the dimer along the hopping pathway 1(3) in molecule 1-2 crystal.

The average electron mobilities at T=300K for the above molecular crystals are calculated by equations (1)～(4) with the reorganization energies and transfer integral data, and the results are also listed in Table 2. Their average hole mobilities are also obtained by the same method in Table S3. It can be found that compared with hole mobilities, these molecular crystals almost possess much larger average electron mobilities within the range $0.67～2.49cm^2V^{-1}s^{-1}$. Coupled with their fine ability of electron injection and high stability of the corresponding organic radical anions, these molecules with pyrazines should be a class of promising candidates for excellent *n*-type OFET materials. It is noted that the calculated electron mobility for molecule 3-7 is remarkably smaller than the experimental largest value, which should be caused by the anisotropic

transport property in organic crystal. Recently, Han et al. have used the following expression to calculate anisotropic carrier mobility:[73]

$$\mu_\Phi = \frac{e}{2k_BT} \sum_i r_i^2 k_i P_i \cos^2 \gamma_i \cos^2 (\theta_i - \Phi) \qquad (9)$$

where θ_i and γ_i are the hopping angles along the specific transistor channel relative to the reference axis. Due to small transfer integral value for the dimer along transfer pathway 4 for molecule 3-7, only three intra-layer (a-b plane) transfer pathways are considered $i.e.$ $\gamma_i=0°$. To compare the differences between their anisotropic mobilities for molecule 3-6 and 3-7 crystals, the values in the a–b plane are calculated. Here, the reference axis is set as the crystallographic b axis, and the orientation angle along the specific conducting channel relative to the reference b axis is Φ (the definitions of the three pathways and Φ are presented in Figure 11, (a) for molecule 3-6 and (b) for 3-7). The results are presented in Figure 11, (c) and (d) for 3-6 and 3-7, respectively. It can be found that the angle Φ dependences of mobilities in 3-6 and 3-7 crystals show remarkable anisotropic behavior, and their respective highest mobility values are 5.46cm^{2}V^{-1}s^{-1} when $\Phi=0°/180°$ and 2.16cm^{2}V^{-1}s^{-1} when Φ is approach to 100°/280°. It should be reason that from Figure 11 (a) and (b), their hopping pathways possessing the maximal transfer integrals are along the above directions. As predicted by us, the calculated maximal anisotropic mobility (2.16cm^{2}V^{-1}s^{-1}) for molecule 3-7 crystal agrees well with the experimental results of 1.0～3.3cm^{2}V^{-1}s^{-1}. In addition, so large mobility in

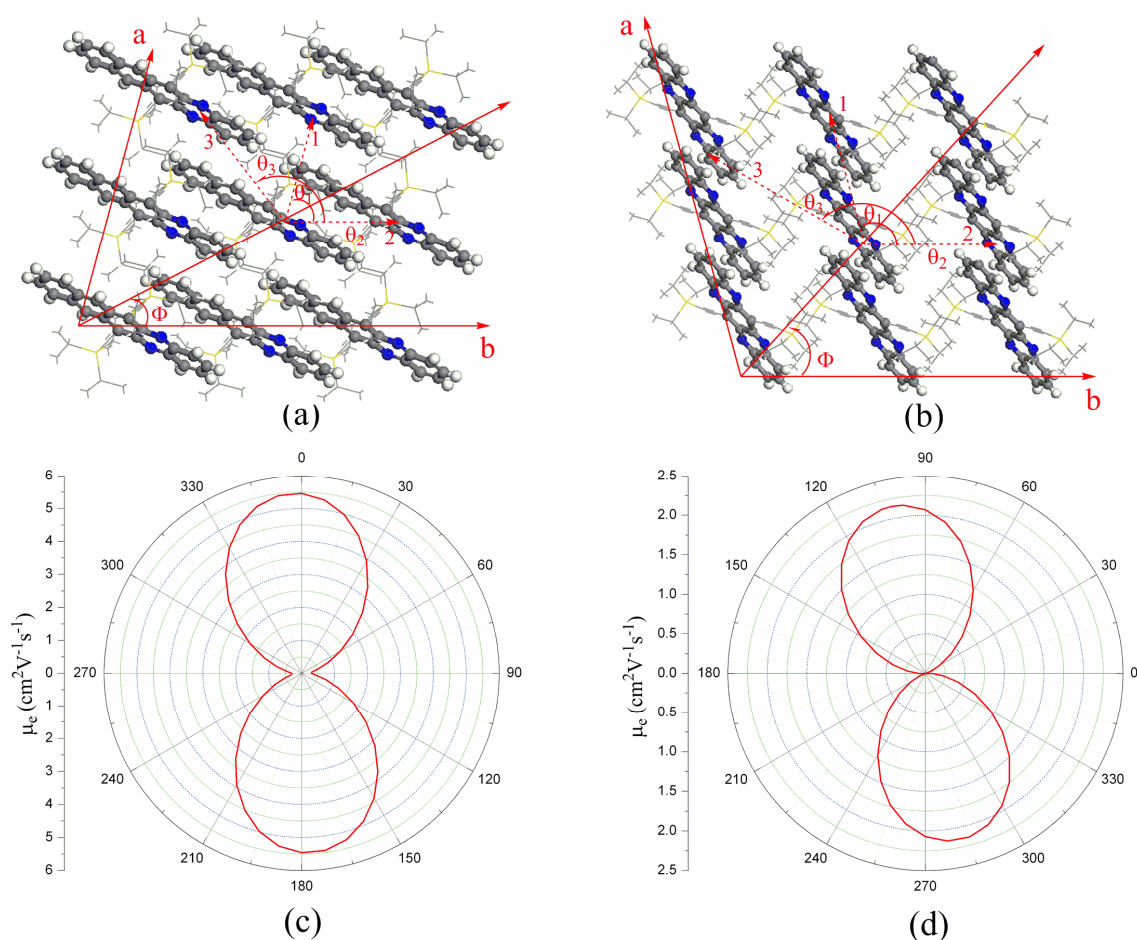the specific direction for molecule 3-6 crystal probably makes it be widely applied to *n*-type OFETs.

Figure 11. (a) and (b): illustration of projecting different hopping pathways to a transistor channel in the a–b plane of 3-6 and 3-7 crystals, respectively. θ1, θ2, and θ3 are the angles of 1, 2, and 3 dimers relative to the reference crystallographic axis b. Φ is the angle along a transistor channel relative to the reference crystallographic axis b; (c) and (d): the curves of the calculated anisotropic mobilities for 3-6 and 3-7, respectively.

Electronic Band Structures. Although the hopping mechanism was used here and the calculated average electron mobilities also agreed well

with the experimental results, in order to further understand on the anisotropy of carrier transport in single crystals, the electronic band structures of the 1-2, 3-6/7 and 6-12/13 crystals were calculated and shown in Figure 12. In general, strongly dispersive bands are seen only in certain regions of the first Brillouin zone; the appearance of both dispersive and flat bands reflects the anisotropic carrier transport properties in the crystals. From Figure 12, the conduction and valence bands of molecules 3-6 and 3-7 don't possess the degenerate character due to the presence of only one molecule in their unit cells. For molecule 1-2, four molecules exist in its unit cell, and two are geometrically inequivalent; as a result, both valence and conduction bands split into sub-bands quasi-degenerate two by two (the sub-band splitting of 117 and 13 meV for the valence and conduction bands, respectively). It is interesting that two degenerate sub-bands exhibit the specific mirror symmetry because two equivalent molecules in its unit cell possess the center symmetry. To further understand the bandwidth variations in the above crystals from the perspective of molecular packing, their band structures are discussed below, in conjunction with the corresponding intermolecular electronic coupling. From Figure 12, the strong conduction band dispersion for molecule 1-2 appears in the GY (the bandwidth of 0.14eV), GA (the bandwidth of 0.15eV) and GC (the bandwidth of 0.14eV) directions, corresponding to the region (transport pathways 1and 3) with large electronic coupling in real space. As analyzed

in the above section, the low-dimension transport character of molecule 3-6 and 3-7 crystals leads to very flat conduction band in the GZ direction. And their largest bandwidths (0.37eV for 3-6; 0.21eV for 3-7) for the conduction band appear in the GA direction, which agrees with the transfer pathway possessing the maximal V value. In the one-dimensional tight-binding model, the bandwidth W can be calculated from the transfer integral V using *W=4V*. Comparing the largest bandwidth estimated (4V=0.41(0.23)eV for molecule 3-6(3-7)) in this way with that (W=0.37(0.21)eV for molecule 3-6(3-7)) directly from the conduction band, so close values also reflect their low-dimension charge transport characters in molecules 3-6 and 3-7 crystals.
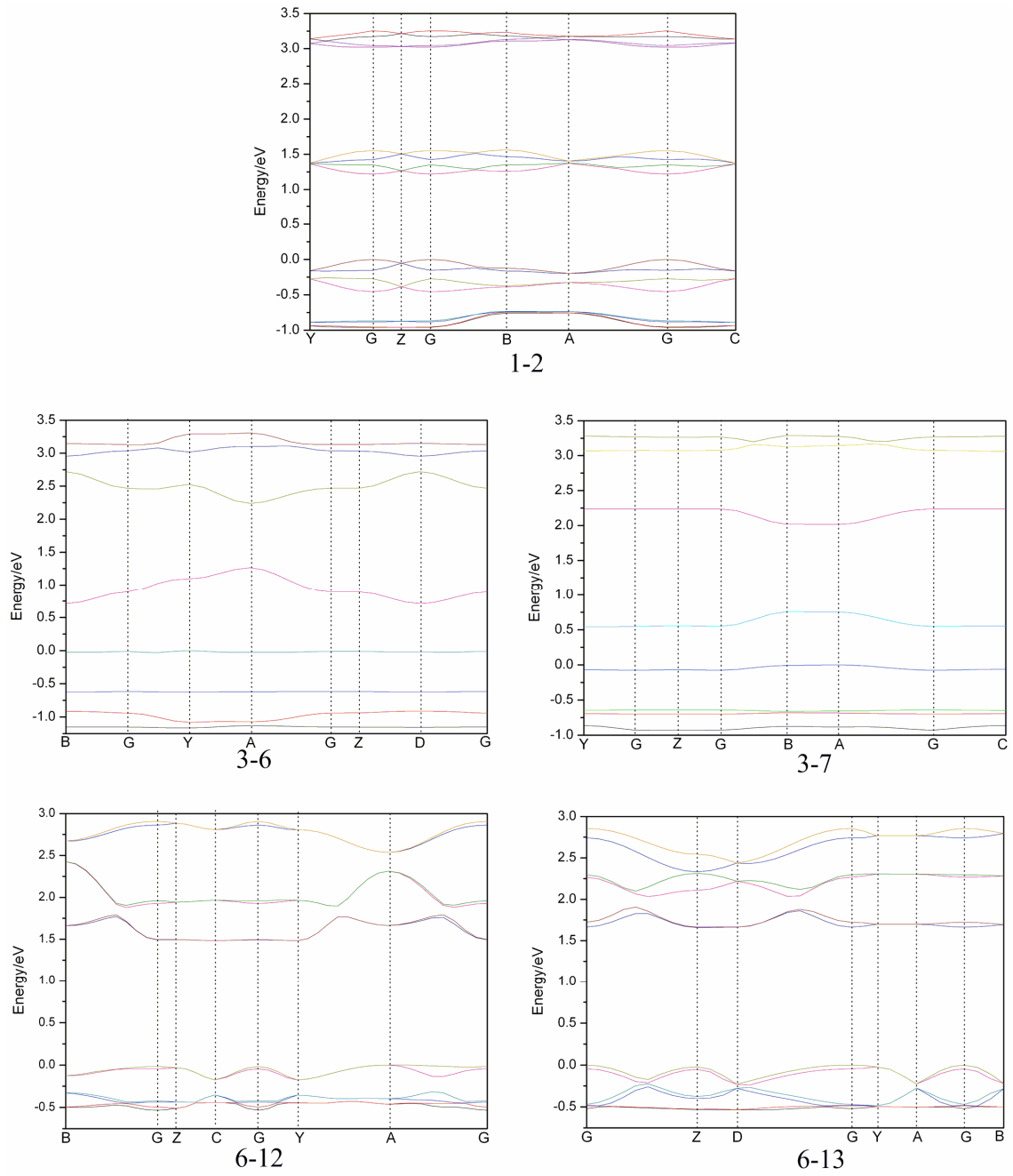
Figure 12. The band structures of the crystals 1-2(*P21/C* space group; a=7.07, b=8.44, c=18.52, α=90°, β=95.23°, γ=90°), 3-6(*P1* space group; a=7.66, b=7.72, c=16.98, α=78.23°, β=88.76°, γ=81.78°), 3-7(*P-1* space group; a=8.06, b=10.51, c=12.76, α=99.83°, β=100.78°, γ=101.53°), 6-12(*P21/N* space group; a=3.89, b=9.07, c=18.43, α=90°, β=92.33°, γ=90°) and 6-13(*C2/M* space group; a=10.59, b=16.04, c=3.8, α=90°, β=95.61°,

γ=90°); Points of high symmetry in the first Brillouin zone are labeled as follows: G(0, 0, 0), B(0.5, 0, 0), Y(0, 0.5, 0), Z(0, 0, 0.5), A(0.5, 0.5, 0), D(0.5, 0, 0.5), C(0, 0.5, 0.5) and E(0.5, 0.5, 0.5).

Conclusions

In the work, their geometrical and electronic structures, molecular stacking motifs, carrier injection and transport properties as well as electronic band structures for the molecules with pyrazines have been detailedly investigated by density functional theory coupled with Marcus electron transfer theory and Brownian diffusion assumption. The results indicate that the introduction of pyrazine doesn't affect the molecular planarity, largely decreases the energies of LUMOs and hence improves their ability of electron injection and their stability in air. Its introduction slightly increases electron reorganization energies by 0.01～0.06eV, which doesn't largely affect their charge transfer rate, and the electron reorganization energies for other molecules studied are below 0.2eV except for series molecules 4. More important, its introduction into molecules 1-1 and 5-10 inverts their herringbone packing into the π-stacking of molecules 1-2 and 5-11 which will give rise to optimal π-orbital overlap, and other studied molecules with pyrazines also exhibit the π-stacking motif. Due to the above advantages, they possess very large average electron mobilities within the range 0.67-2.49cm^{2}V^{-1}s^{-1}, which makes them a class of

promising candidates for excellent *n*-type OFET materials. So introducing pyrazine is an effective approach to obtain the excellent n-type OFET materials. The studies on the structure-property relations can provide a fertile theoretical ground with the rational molecular design and synthesis of the desired *n*-type OFET materials.

Supporting Information Available: Figure S1, the absolute values of bond lengths changes between the neutral and ionized geometries for series molecules 3 and 6; Table S1, giving HOMO and LUMO energies (E_{HOMO} and E_{LUMO}), ionization potentials (IPs), electronic affinities (EAs) of their dimers and monomers for molecules 6-12 and 6-13 obtained by M06-2X/6-31+G(d,p); Table S2, giving HOMO and LUMO energies (E_{HOMO} and E_{LUMO}), ionization potentials (IPs), electronic affinities (EAs), extraction potentials and reorganization energies (λs) of tetracene derivative with pyridine; Table S3, giving average hole mobilities for the crystal structures of the studied molecules with pyrazine.

References and Notes

(1) Tang, C. W.; Van Slyke, S. A. *Appl. Phys. Lett*. **1987**, 51, 913.

(2) Ho, P. K. H.; Kim, J.-S.; Burroughes, J. H.; Becker, H.; Li, S. F. Y.; Brown, T. M.; Cacialli, F.; Friend, R. H. *Nature* **2000**, 404, 481.

(3) Katz, H. E. *J. Mater. Chem.* **1997**, 7, 369.

(4) Horowitz, G.; Hajlaoui, M. E. *Adv. Mater.* **2000**, 12, 1046.

(5) Newman, C. R.; Frisbie, C. D.; da Silva Filho, D. A.; Brédas, J. L.; Ewbank, P. C.; Mann, K. R. *Chem. Mater.* **2004**, 16, 4436.

(6) Padinger, F.; Rittberger, R. S.; Sariciftci, N. S. *Adv. Funct. Mater*. **2003**, 13, 85.

(7) Brabec, C. J.; Sariciftci, N. S.; Hummelen, J. C. *Adv. Funct. Mater*. **2001**, 11, 15.

(8) Sundar, V. C.; Zaumseil, J.; Podzorov, V.; Menard, E.; Willett, R. L.; Someya, T.; Gershenson, M. E.; Rogers, J. A. *Science* (Washington, D. C, U.S.) **2004**, 303,1644.

(9) Podzorov, V.; Menard, E.; Borissov, A.; Kiryukhin, V.; Rogers, J. A.; Gershenson, M. E. *Phys. Rev. Lett.* **2004**, 93, 86602.

(10) DeLongchamp, D. M.; Kline, R. J.; Lin, E. K.; Fischer, D. A.; Richter, L. J.; Lucas, L. A.; Heeney, M.; McCulloch, I.; Northrup, J. E. *Adv. Mater.* **2007**, 19, 833.

(11) Zhang, M.; Tsao, H. N.; Pisula, W.; Yang, C.; Mishra, A. K.; Muellen, K. *J. Am. Chem. Soc.* **2007**, 129, 3472.

(12) Huang, C.; West, J. E.; Katz, H. E. *Adv. Funct. Mater*. **2007**, 17,

142.

(13) Anthony, J. E. *Chem. Rev.* **2006**, 106, 5028.

(14) Kastler, M.; Laquai, F.; Mullen, K.; Wegner, G. *Appl. Phys. Lett.* **2006**, 89, 252103/1.

(15) Naraso; N, J.-I.; Kumaki, D.; Tokito, S.; Yamashita, Y. *J. Am. Chem. Soc.* **2006**, 128, 9598.

(16) Chabinyc, M. L.; Salleo, A.; Wu, Y.; Liu, P.; Ong, B. S.; Heeney, M.; McCulloch, I. *J. Am. Chem. Soc.* **2004**, 126, 13928.

(17) Reese, C.; Bao, Z. *Mater. Today* **2007**, 10, 20.

(18) Briseno, A. L.; Mannsfeld, S. C. B.; Ling, M. M.; Liu, S.; Tseng, R. J.; Reese, C.; Roberts, M. E.; Yang, Y.; Wudl, F.; Bao, Z. *Nature* **2006**, 444, 913.

(19) Murphy, A. R. ; Fréchet, J. M. *Chem. Rev.* **2007**, 107 , 1066

(20) Jones, B. A.; Ahrens, M. J.; Yoon, M. H.; Facchetti, A.; Marks, T. J.; Wasielewski, M. R. *Angew. Chem.* **2004**, 116, 6523; *Angew. Chem. Int. Ed.* **2004**, 43, 6363

(21) Wang, Z.; Kim, C.; Facchetti, Antonio; Marks, T. J. *J. Am. Chem. Soc.* **2007**, 129, 13362.

(22) Hutchison. G. A.; Ratner, M. A; Marks, T. J. *J. Am. Chem. Soc.* **2005**, 127, 2339.

(23) Kuo, M.-Y.; Chen H.-Y.; Chao, I. *Chem. Eur. J.* **2007**, 13, 4750.

(24) Sakamoto, Y.; Suzuki, T.; Kobayashi, M.; Gao, Y.; Fukai, Y.; Inoue,

Y.; Sato, F.; Tokito, S. *J. Am. Chem. Soc.* **2004**, 126, 8138.

(25) Inoue, Y.; Sakamoto, Y.; Suzuki, T.; Kobayashi, M.; Gao, Y.; Tokito, S. *Jpn. J. Appl. Phys., Part 1* **2005**, 44, 3663.

(26) Sakamoto, Y.; Suzuki, T.; Kobayashi, M.; Gao, Y.; Inoue, Y.; Tokito, S. *Mol. Cryst. Liq. Cryst.* **2006**, 444, 225.

(27) Sancho-GarcÍa, J. C; Pérez-Jiménez, A. J.; Olivier, Y.; Cornil, J. *Phys. Chem. Chem. Phys.*, **2010**, 12, 9381

(28) Geng, Y.; Wang, J.; Wu, S.; Li, H.; Yu, F.; Yang, G.; Gao, H.; Su, Z. *J. Mater. Chem.*, **2011**, 21, 134

(29) Bunz, U. H. F. *Chem. Eur. J.* **2009**, 15, 6780.

(30) Miao, S.; Brombosz, S. M.; Schleyer P. v. R.; Wu, J. I.; Barlow, S.; Marder, S. R.; Hardcastle, K. I.; Bunz, U. H. F. *J. Am. Chem. Soc.* **2008**, 130, 7339

(31) Nakagawa, T.; Kumaki, D.; Nishida, J.-i.; Tokito, S.; Yamashita, Y.; *Chem. Mater.* **2008**, 20, 2615

(32) Naraso; Nishida, J.-i.; Ando, S.;, Yamaguchi, J.; Itaka, K.; Koinuma, H.; Tada, H.; Tokito, S.; Yamashita, Y. *J. Am. Chem. Soc.* **2005**, 127, 10142

(33) Liang, Z.; Tang, Q.; Xu, J.; Miao, Q. *Adv. Mater.* **2011**, 23, 1535

(34) Tang, Q.; Liang, Z.; Liu, J.; Xu, J.; Miao, Q. *Chem. Commun.*, **2010**, 46, 2977

(35) Liang, Z.; Tang, Q.; Liu, J.; Li, J.; Yan, F.; Miao, Q. *Chem. Mater.*

2010, 22, 6438

(36) Winkler, M.; Houk, K. N. *J. Am. Chem. Soc.* **2007**, 129, 1805

(37) Sun, Y.; Liu, Y.; Zhu, D.; *J. Mater Chem.* **2005**, 15, 53.

(38) Tauber, M. J.; Kelley, R. F.; Giaimo, J. M.; Rybtchinski, B; Wasielewski, M. R. *J. Am. Chem. Soc*., **2006**, 128, 1782.

(39) Bredas, J. L.; Beljonne, D.; Coropceanu, V.; Cornil, J. *Chem. Rev.*, **2004**, 104, 4971.

(40) Yang, X. D.; Wang, L. J.; Wang, C. L.; Long, W.; Shuai, Z. G. *Chem. Mater.* **2008**, 20, 3205.

(41) Yang, X. D.; Li, Q. K.; Shuai, Z. G. *Nanotechnology*. **2007**, 18, 424029.

(42) Coropceanu, V.; Cornil, J.; da Silva Filho, D. A.; Olivier, Y.; Silbey, R.; Brédas, J. L. *Chem. Rev.* **2007**, 107, 926.

(43) Nam, M. S.; Ardavan, A.; Cava, R. J.; Chaikin, P. M. *Appl. Phys. Lett.* **2003**, 83, 4782.

(44) de Boer, R. W. I.; Jochemsen, M.; Klapwijk, T. M.; Morpurgo, A. F.; Niemax, J.; Tripathi, A. K.; Pflaum, J. *J. Appl. Phys.* **2004**, 95, 1196.

(45) Mott, N. F.; Davis, E. A. *Electronic Process Non-Crystalline Materials*, 2d ed.; Oxford University Press: Oxford, **1979**.

(46) Epstein, A. J.; Lee, W. P.; Prigodin, V. N. *Synth. Met*. **2001**, 117, 9.

(47) Marcus, R. A. *Rev. Mod. Phys.* **1993**, 65, 599.

(48) Schein, L. B.; McGhie, A. R. *Phys. Rev. B: Condens. Matter Mater.*

Phys. **1979**, 20, 1631.

(49) Li, C.-H.; Huang C.-H.; Kuo, M.-Y. *Phys. Chem. Chem. Phys.*, **2011**, 13, 11148

(50) Delgado, M. C. R.; Kim, E.-G.; da Silva Filho, D. A.; Brédas, J.-L. *J. Am. Chem. Soc.* **2010**, 132, 3375

(51) Frisch, M. J.; Trucks, G. W.; Schlegel, H. B.; Scuseria, G. E.; Robb, M. A.; Cheeseman, J. R.; Montgomery, J. A., Jr.; Vreven, T.; Kudin, K. N.; Burant, J. C.; Millam, J. M.; Iyengar, S. S.; Tomasi, J.; Barone, V.; Mennucci, B.; Cossi, M.; Scalmani, G.; Rega, N.; Petersson, G. A.; Nakatsuji, H.; Hada, M.; Ehara, M.; Toyota, K.; Fukuda, R.; Hasegawa, J.; Ishida, M.; Nakajima, T.; Honda, Y.; Kitao, O.; Nakai, H.; Klene, M.; Li, X.; Knox, J. E.; Hratchian, H. P.; Cross, J. B.; Bakken, V.; Adamo, C.; Jaramillo, J.; Gomperts, R.; Stratmann, R. E.; Yazyev, O.; Austin, A. J.; Cammi, R.; Pomelli, C.; Ochterski, J. W.; Ayala, P. Y.; Morokuma, K.; Voth, G. A.; Salvador, P.; Dannenberg, J. J.; Zakrzewski, V. G.; Dapprich, S.; Daniels, A. D.; Strain, M. C.; Farkas, O.; Malick, D. K.; Rabuck, A. D.; Raghavachari, K.; Foresman, J. B.; Ortiz, J. V.; Cui, Q.; Baboul, A. G.; Clifford, S.; Cioslowski, J.; Stefanov, B. B.; Liu, G.; Liashenko, A.; Piskorz, P.; Komaromi, I.; Martin, R. L.; Fox, D. J.; Keith, T.; Al.Laham, M. A.; Peng, C. Y.; Nanayakkara, A.; Challacombe, M.; Gill, P. M. W.; Johnson, B.; Chen, W.; Wong, M. W.; Gonzalez, C.; Pople, J. A. *Gaussian 09*, revision A.02; Gaussian, Inc.: Wallingford, CT, 2009.

(52) Senthilkumar, K.; Grozema, F. C.; Bickelhaupt, F. M.; Siebbeles, L. D. A. *J. Chem. Phys.* **2003**, 119, 9809–9817.

(53) Valeev, E. F.; Coropceanu, V.; da Silva, D. A.; Salman, S.; Brédas, J. L. *J. Am. Chem. Soc.* **2006**, 128, 9882–9886.

(54) Huang, J. S.; Kertesz, M. *J. Chem. Phys.* **2005**, 122, 234701.

(55) Velde, G. T.; Bickelhaupt, F. M.; Baerends, E. J.; Guerra, C. F.; Van Gisbergen, S. J. A.; Snijders, J. G.; Ziegler, T. *J. Comput. Chem.* **2001**, 22, 931.

(56) Perdew, J. P.; Burke, K.; Ernzerhof, M. *Phys. Rev. Lett.* **1996**, 77, 3865.

(57) Delley, B. *J. Chem. Phys.* **1990**, 92, 508.

(58) Delley, B. *J. Chem. Phys.* **2000**, 113, 7756.

(59) Monkhorst, H. J.; Pack, J. D. *Phys. ReV. B* **1977**, 16, 1748.

(60) Zade, S. S.; Bendikov, M. *Chem.—Eur. J.* **2008**, 14, 6734.

(61) Wen, Y.; Liu, Y. *Adv. Mater.* **2010**, 22, 1331.

(62) Liu, H.; Kang, S.; Lee, J. Y. *J. Phys. Chem. B* **2011**, 115, 5113.

(63) Norton, J. E.; Bredas, J. L. *J. Am. Chem. Soc.*, **2008**, 130, 12377.

(64) Liu, H.; Mu, J.; Lee, J. Y. *J. Phys. Chem. B* **2011**, 113, 8409.

(65) Koh, S. E.; Risko, C.; da Silva, D. A.; Kwon, O.; Facchetti, A.; Bredas, J. L.; Marks, T. J; Ratner, M. A. *Adv. Funct. Mater.* **2008**, 18, 332.

(66) Norton, J. E.; Bredas, J. L. *J. Chem. Phys.*, **2008**, 128, 034701.

(67) Bredas, J. L.; Calbert, J. P.; da Silva, D. A.; Cornil, J. *Proc. Natl.*

Acad. Sci. U. S. A., **2002**, 99, 5804.

(68) Anthony, J. E.; Brooks, J. S.; Eaton, D. L.; Parkin, S. R. *J. Am. Chem. Soc.* **2001**, 123, 9482

(69) Anthony, J. E.; Eaton, D. L.; Parkin, S. R. *Org. Lett.*, **2002**, 4, 15.

(70) Vura-Weis, J.; Ratner, M. A.; Wasielewski, M. R. *J. Am. Chem. Soc* **2010**, 132, 1738.

(71) Jacquemin, D. Perpète, E. A.; Ciofini, I.; Adamo, C.; Valero, R.; Zhao, Y.; D. Truhlar, G. *J. Chem. Theory. Comput.* **2010**, 6, 2071.

(72) Tauer, T. P.; Sherrill, C. D. *J. Phys. Chem. A* **2005**, 109, 10475

(73) Huang J.-D.; Wen, S.-H.; Deng, W.-Q.; Han, K.-L. *J. Phys. Chem. B* **2011**, 115, 2140.

Supporting Information

for

A Promising Approach to Obtain Excellent n-Type Organic Field-Effect Transistors — Introducing Pyrazine Ring

Xian-Kai Chen,[†] Jing-Fu Guo,[‡] Lu-Yi Zou,[†] Ai-Min Ren[*,†] and Jian-Xun Fan[†]

† *State Key Laboratory of Theoretical and Computational Chemistry, Institute of Theoretical Chemistry, Jilin University, Changchun 130023, China*
‡ *School of Physics, Northeast Normal University, 130024, P. R. China*
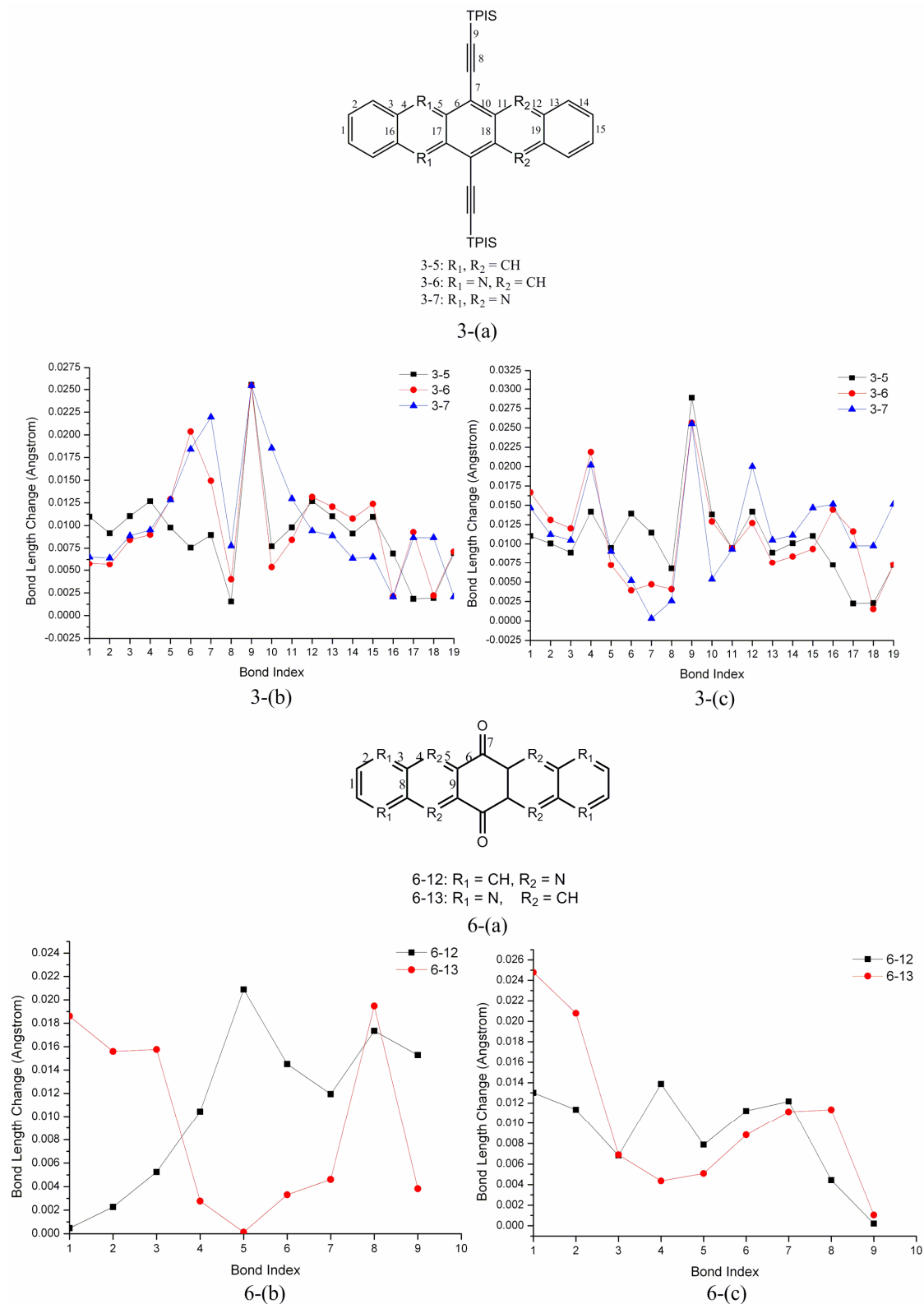*Correspondence to:* A.-M. Ren; e-mail: **aimin_ren@yahoo.com**

Figure S1. (a) The bond index of the bond lengths; the absolute values of bond length changes between the neutral and ionized geometries, (b) for hole and (c) for electron. The prefixion 3 and 6 denote series molecules 3

and 6, respectively.

Table S1. HOMO and LUMO Energies (E_{HOMO} and E_{LUMO}), Ionization Potentials (IPs), Electronic Affinities (EAs) of their Dimers and Monomers for Molecules 6-12 and 6-13 Obtained by M06-2X/6-31+G(d,p). (in eV)

species	E_{HOMO}	E_{LUMO}	IP(v)	EA(v)
Dimer(6-12)	-8.54	-2.82	9.11	2.39
Dimer(6-13)	-8.75	-2.79	9.20	2.30
Monomer(6-12)	-8.66	-2.67	9.47	2.05
Monomer(6-13)	-8.74	-2.47	9.80	1.81

On the basis of the geometry of the monomer, some parameters calculated, such as HOMO and LUMO energies, IP, EA, EEP, HEP, as well as the reorganization energy, reflect some intrinsic characters at the single-molecule level, and some molecular materials possessing fine performance can be distinguished by these characters. So the intermolecular interactions aren't taken into account in the calculations of these characters. On the other hand, to understand the effects of the intermolecular interactions on these parameters, molecules 6-12 and 6-13 are taken as the examples and compared. The dimers (the dimer 1 for molecules 6-12 and 6-13 in Table 2) possessing the shortest mass center distances in their crystal structures are optimized by employing M06-2X/6-31+G(d,p), and the corresponding HOMO and LUMO energies, IP(v) and EA(v) values for the dimers are obtained in Table S1. Bredas JL et al have shown that external reorganization energy is small relative to

internal value in the literature (*J. Am. Chem. Soc.* 2008, 130, 12377–12384), so the polarization effects from the surrounding molecules on the reorganization energy aren't taken into account here. For the optimized dimers, the mass central distances between the monomers slightly decrease. For comparing these values of the dimers with ones of the corresponding monomers, these parameters for 6-12 and 6-13 monomers are also calculated by the same methods and the results are also listed in Table S1. From the table, the differences of the above values between the dimers and corresponding monomers are similar to the case reported in the literatures (*J. Phys. Chem. B* **2011**, 115, 5113). It can be found that the relative orders of the values obtained by M06-2X/6-31+G(d,p) for the dimers and monomers are accordant, and the orders are also consistent with the relative orders of these values for the monomers in the main article. So the intermolecular interactions should possess little effect on evaluating the relative performances of these molecular materials by the above parameters obtained at single-molecule level.

Table S2. HOMO and LUMO Energies (E_{HOMO} and E_{LUMO}), Ionization Potentials (IPs), Electronic Affinities (EAs), Extraction Potentials and Reorganization Energies (λs) of Tetracene Derivative with Pyridine (in eV)

Species	E_{HOMO}	E_{LUMO}	IP(v)	IP(a)	HEP	EA(v)	EA(a)	EEP	λ_{hole}	λ_{elec}
a	-5.20	-2.37	6.91	6.85	6.80	1.27	1.36	1.44	0.11	0.17

To further explain why the 2nd N atom of pyrazine is introduced, its frontier molecular orbitals, IP, EA and reorganization energies for tetracene derivative with pyridine (*a* in the following Figure) are calculated and are compared with those of molecule 1-2, and the results are listed in Table S2. It can be found that the 2nd N atom introduced plays a dominant role in stabilizing the HOMO and LUMO levels of the molecule, which should be beneficial for reducing the electron injection barrier. Due to its introduction, the increase of EA value enhances the stability of n-type OFETs composed of molecule 1-2. In the meantime, the reorganization energies of molecules 1-2 and *a* have little change. So the introduction of the 2nd N atom is very necessary. And the problem has been detailedly discussed in the literature (*J. Am. Chem. Soc.* **2007**, 129, 1805)
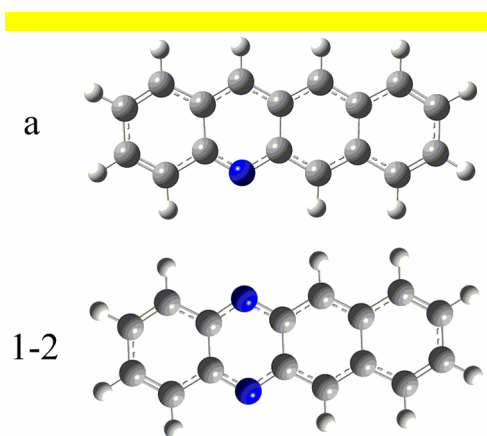

Table S3. Average hole mobilities (μ_{hole}) for the crystal structures of the studied molecules with pyrazine. ($cm^2V^{-1}s^{-1}$)

species	1-2	3-6	3-7	6-12	6-13
μ_{hole}	1.29	0.0044	0.046	0.029	0.11